Berry curvature for coupled waves of magnons and electromagnetic waves

Akihiro Okamoto,[1] Ryuichi Shindou,[2,3] and Shuichi Murakami[1]
[1]*Department of Physics, Tokyo Institute of Technology, 2-12-1 Ookayama, Meguro-ku, Tokyo 152-8551, Japan*
[2]*International Center for Quantum Materials, School of Physics, Peking University, Beijing 100871, China*
[3]*Collaborative Innovation Center of Quantum Matter, Beijing 100871, China*

(Received 30 April 2020; revised 23 July 2020; accepted 3 August 2020; published 20 August 2020)

In this paper, we introduce Berry curvature, topological Chern number, and topological chiral edge mode that emerge from a hybridization between magnon and electromagnetic wave in a ferromagnet insulator. By focusing on the energy conservation, we first reformulate the Landau-Lifshitz-Maxwell equation into a Hermitian eigenvalue equation. From the eigenvalue equation, we define the Berry curvature of the magnon-photon coupled waves. We show that the Berry curvature thus introduced shows a prominent peak around a hybridization point between magnon mode and photon mode, and a massive hybrid mode takes a nonzero Chern number (± 1) due to the magnon-photon coupling. In accordance with the nonzero Chern number, the topological edge modes emerge inside the hybridization gap at a domain wall between two ferromagnetic insulators with opposite magnetizations.

DOI: 10.1103/PhysRevB.102.064419

I. INTRODUCTION

Coupled waves between ferromagnetic moments and electromagnetic waves have been studied for a long time. Dispersion relations of the coupled waves of the magnon and the electromagnetic wave in layered film structures consisting of magnetic, ferroelectric, and insulating layers are studied theoretically [1–3] and experimentally. In recent years, coupling between quantum spins and photons have attracted much attention both in theory and in experiment. The coupled wave of spins and photons behaves differently depending on the strength of the coupling. When the coupling is strong, the wave is called a magnon polariton [4,5]. The magnon polariton is promising for applications in quantum information science and technology. Recently, strong coupling between the Kittel mode and the cavity mode is studied in the YIG sphere [6–8], film [9], and film split rings [10].

The Berry curvature in various physical systems has also been attracting many researchers. A geometric character of the Bloch wave function gives rise to new phenomena such as topological electric and thermal Hall effect [11]. The Berry curvature have been studied in electrons [12,13], photons [14–19], magnons [20–26], and so forth. Recently, calculations of finite Berry curvature are reported in various coupled systems such as systems with charge density and current coupling [27,28], exciton-photon coupling [29], and magnon-phonon coupling [30–34]. The hybridizations among these degrees of freedom lead to topological bands and novel edge states inside a hybridization gap. In the previous work, we have calculated the Berry curvature of magnetoelastic wave by formulating a Hermitian eigenvalue equation from an equation of motion for the magnetoelastic wave [35].

In this paper, we formulate a Hermitian eigenvalue equation for coupled equations of motion for ferromagnetic moments and electromagnetic waves. Based on the formulation, we calculate the Berry curvature of the coupled waves of magnons and electromagnetic waves [36]. We find that the Berry curvature is prominently enhanced at a crossing point of the dispersions and we clarify its asymptotic behavior around the crossing point. We find that in the presence of the finite hybridization, the topological Chern number of the coupled wave becomes quantized to be nonzero integer. We show that in accordance with the nonzero Chern number, nontrivial topological edge modes of the coupled wave appear inside the hybridization gap at a domain wall.

This paper is organized as follows. In Sec. II, we formulate generalized Hermitian eigenvalue equations from the equations of motion of magnons and electromagnetic waves and calculate eigenfrequencies. In Secs. III and IV, we calculate the Berry curvature, the Chern number, and its edge modes of the magnon and electromagnetic waves. We summarize the paper in Sec. V.

II. FORMULATION OF EIGENVALUE EQUATION

We consider a three-dimensional ferromagnetic insulator with isotropic electric permittivity. The saturation magnetization $\boldsymbol{M}_0$ and the applied magnetic field $\boldsymbol{H}_0$ are parallel to each other, and they are along the z direction. The magnon field is described by a magnetization $\boldsymbol{m}$ in the xy plane (Fig. 1). We assume that electromagnetic waves with the magnetic flux density $\boldsymbol{b}$ and the electric field $\boldsymbol{e}$ transmit entirely through the ferromagnetic insulator without dissipation. The amplitudes of the magnon and the electromagnetic waves are proportional to $\exp i(\boldsymbol{k}\cdot r - \omega t)$, with frequency ω and wave vector $\boldsymbol{k} \equiv (k_x, k_y, k_z) \equiv k(\sin\theta\cos\varphi, \sin\theta\sin\varphi, \cos\theta)$ (Fig. 1). Therefore, θ represents an angle between the wave vector and the saturation magnetization. The coupled equations of

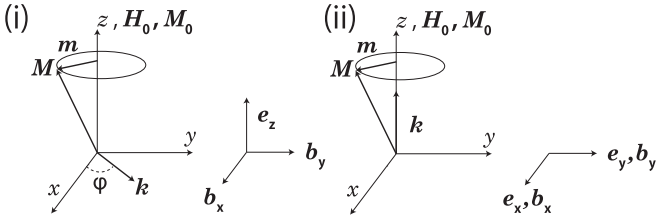

FIG. 1. Schematic illustration of the magnons and the electromagnetic waves for (i) the wave vector perpendicular to the saturation magnetization ($\theta = \pi/2$) and (ii) the wave vector parallel to the saturation magnetization $\theta = 0$ (in Appendix A).

motions (EOM) consist of the Landau-Lifshitz equation and the Maxwell equation [36,37]. In terms of the wave vector $\boldsymbol{k}$, the EOM take forms of

$$\frac{\partial m_x}{\partial t} = \frac{\omega_M}{4\pi} b_y - \omega_s m_y, \tag{1}$$

$$\frac{\partial m_y}{\partial t} = -\frac{\omega_M}{4\pi} b_x + \omega_s m_x, \tag{2}$$

$$\frac{\partial \boldsymbol{b}}{\partial t} = -icK\boldsymbol{e}, \tag{3}$$

$$\frac{\partial \boldsymbol{e}}{\partial t} = i\frac{cK}{\epsilon}(\boldsymbol{b} - 4\pi \boldsymbol{m}), \tag{4}$$

where $\omega_s \equiv \omega_M + \omega_H$, $\omega_M \equiv 4\pi g M_0$, $\omega_H \equiv g H_0$, g is gyromagnetic constant, c is the speed of light, ϵ is the permittivity, and K is an antisymmetric matrix defined as

$$K = \begin{pmatrix} 0 & -k_z & k_y \\ k_z & 0 & -k_x \\ -k_y & k_x & 0 \end{pmatrix}. \tag{5}$$

For the later convenience, let us express Eqs. (1)–(4) as

$$i\frac{\partial}{\partial t}\boldsymbol{x_k} = H_{\rm eff}\boldsymbol{x_k}, \tag{6}$$

where $\boldsymbol{x_k}$ is the eigenvector, $\boldsymbol{x_k} = {}^t(m_{\boldsymbol{k},x}, m_{\boldsymbol{k},y}, \boldsymbol{b_k}, \boldsymbol{e_k})$. The 8×8 matrix $H_{\rm eff}$ is given by

$$H_{\rm eff} = \begin{pmatrix} \omega_s\sigma_2 & -\frac{\omega_M}{4\pi}\sigma_2' & 0 \\ 0 & 0 & cK \\ -\frac{4\pi c}{\epsilon}(K')^t & -\frac{c}{\epsilon}K & 0 \end{pmatrix} \tag{7}$$

with a 2×2 matrix σ_2 and 2×3 matrices I', σ_2', K':

$$I' = \begin{pmatrix} 1 & 0 & 0 \\ 0 & 1 & 0 \end{pmatrix}, \tag{8}$$

$$\sigma_2 = \begin{pmatrix} 0 & -i \\ i & 0 \end{pmatrix}, \quad \sigma_2' = \begin{pmatrix} 0 & -i & 0 \\ i & 0 & 0 \end{pmatrix}, \tag{9}$$

$$K' = \begin{pmatrix} 0 & -k_z & k_y \\ k_z & 0 & -k_x \end{pmatrix}. \tag{10}$$

We call $H_{\rm eff}$ an effective Hamiltonian.

To define the Berry curvature for the coupled wave from the EOM, let us assume that a constant Hermitian matrix γ makes $H_{\rm eff}$ to be Hermitian as $\tilde{H}_{\rm eff} \equiv \gamma H_{\rm eff} = \tilde{H}_{\rm eff}^\dagger$. In terms of these Hermitian matrices, the coupled EOM reduces to

$$i\gamma\frac{\partial \boldsymbol{x_k}}{\partial t} = \tilde{H}_{\rm eff}\boldsymbol{x_k}. \tag{11}$$

Define a 'norm' of $\boldsymbol{x_k}$ in terms of the Hermitian matrix γ as $\boldsymbol{x_k}^\dagger\gamma\boldsymbol{x_k}$. Since γ and $\tilde{H}_{\rm eff}$ are both Hermitian, one can see that the norm is a constant of motion, $\partial(\boldsymbol{x_k}^\dagger\gamma\boldsymbol{x_k})/\partial t = 0$. Physically speaking, the constant of motion must correspond to a total energy density of the system. Thus, we choose the Hermitian matrix γ as

$$\gamma = \begin{pmatrix} \frac{(4\pi)^2\omega_s}{\omega_M} I & -4\pi I' & 0 \\ -4\pi(I')^t & I & 0 \\ 0 & 0 & \epsilon I \end{pmatrix}, \tag{12}$$

with

$$\tilde{H}_{\rm eff}(\boldsymbol{k}) = \gamma H_{\rm eff}(\boldsymbol{k}) = \begin{pmatrix} \frac{(4\pi\omega_s)^2}{\omega_M}\sigma_2 & -4\pi\omega_s\sigma_2' & -4\pi cK' \\ -4\pi\omega_s(\sigma_2')^\dagger & \omega_M\Sigma_2 & cK \\ -4\pi c(K')^t & -cK & \boldsymbol{0} \end{pmatrix}, \tag{13}$$

and a 3 by 3 matrix Σ_2,

$$\Sigma_2 = \begin{pmatrix} 0 & -i & 0 \\ i & 0 & 0 \\ 0 & 0 & 0 \end{pmatrix}. \tag{14}$$

Then, the norm is equal to the total energy density, consisting of the energy density of the electric wave u_e and that of the magnetic wave u_m [38–40],

$$\boldsymbol{x_k}^\dagger\gamma\boldsymbol{x_k} = u_e + u_m, \tag{15}$$

$$u_e = \boldsymbol{e_k}^\dagger\frac{\partial(\omega\hat{\epsilon})}{\partial\omega}\boldsymbol{e_k} = \epsilon|\boldsymbol{e_k}|^2, \tag{16}$$

$$u_m = \boldsymbol{h_k}^\dagger\frac{\partial(\omega\hat{\mu})}{\partial\omega}\boldsymbol{h_k} = (4\pi)^2\frac{\omega_H}{\omega_M}|\boldsymbol{m_k}|^2 + |\boldsymbol{h_k}|^2. \tag{17}$$

Here $\hat{\epsilon}$ and $\hat{\mu}$ are an isotropic permittivity tensor and permeability tensor defined by $\boldsymbol{b_k} = \hat{\mu}\boldsymbol{h_k}$ where $\boldsymbol{h_k}$ represents a magnetic field. We henceforth choose a normalization condition of the eigenvector $\boldsymbol{x_k}$ as $\boldsymbol{x_k}^\dagger\gamma\boldsymbol{x_k} = 1$.

The eigenvalue equation (11) gives an equation for the dispersion relation

$$\omega^6 - \left(2\omega_{em}^2 + \omega_s^2\right)\omega^4 + \omega_{em}^2\left(\omega_{em}^2 + 2\omega_H\omega_s + \omega_M\omega_s\sin^2\theta\right)\omega^2 - \omega_H\omega_{em}^4(\omega_H + \omega_M\sin^2\theta) = 0, \tag{18}$$

where $\omega_{em} = ck/\sqrt{\epsilon}$. The dispersion relation in Eq. (18) has only six solutions, while the dimension of the eigenvalue equation (6) is eight. The other two are nothing but two zero modes that correspond to unphysical gauge degrees of freedom. Namely, Eqs. (3) and (4) satisfy $\boldsymbol{k}\cdot\boldsymbol{b} = 0$ and $\boldsymbol{k}\cdot\boldsymbol{e} = 0$, respectively and correspondingly, Eq. (6) always has two eigenvectors that belong to the zero eigenfrequency. The six physical solutions consist of pairs of positive and negative frequencies.

In the following, we only consider the case of (i) $\theta = \pi/2$ as shown in Fig. 1(i). We leave the case of (ii) $\theta = 0$ in Appendix A.

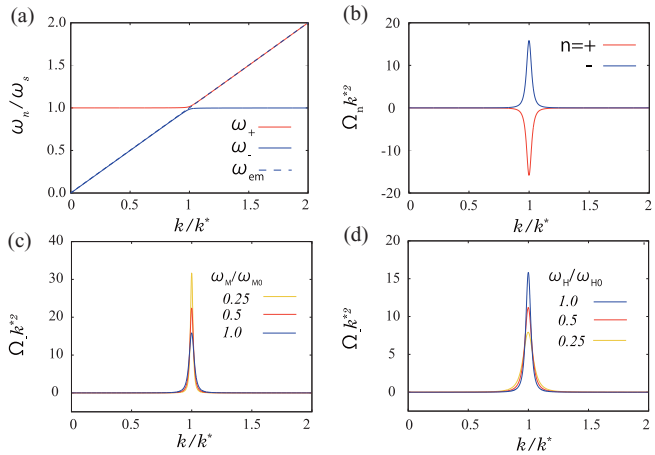

FIG. 2. Dispersions and Berry curvatures for coupled modes between magnons and electromagnetic waves in a weak coupling regime. (a) Dispersions of the ω_+ and ω_- branches and (b) Berry curvatures of the ω_+ and ω_- branches as functions of k. The parameters are set to be $\omega_H/\omega_M = 10^3$ with $\omega_H = 5$ [GHz]. Berry curvatures for the ω_- mode is shown for (c) $\omega_M/\omega_{M0} = 0.25, 0.5, 1.0$ with $\omega_H/\omega_{H0} = 1.0$, and (d) $\omega_H/\omega_{H0} = 0.25,\ 0.5,\ 1.0$ with $\omega_M/\omega_{M0} = 1.0$, with $\omega_{M0} = 5 \times 10^{-3}$ [GHz] and $\omega_{H0} = 5$ [GHz].

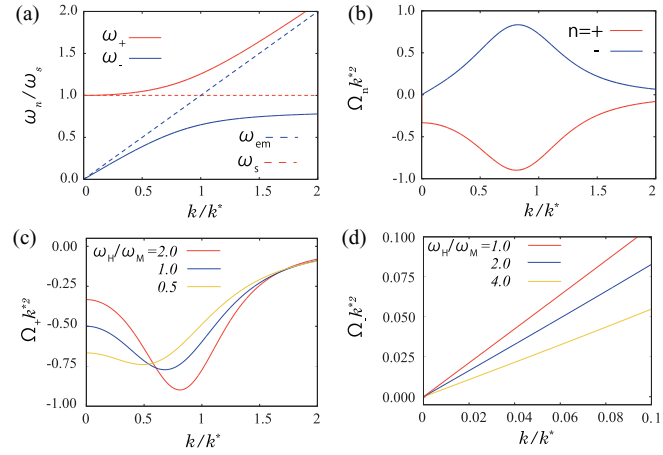

FIG. 3. Dispersions and Berry curvatures for coupled modes between magnons and electromagnetic waves in strong coupling regime. (a) Dispersions of the ω_+ and ω_- branches. (b) Berry curvatures of the ω_+ and ω_- branches as functions of k. $\omega_H/\omega_M = 2.0$ with $\omega_H = 5.0$ (GHz). The Berry curvature of the ω_+ mode is shown for (c) $\omega_H/\omega_M = 0.5, 1.0, 2.0$, and the ω_- mode for (d) $\omega_H/\omega_M = 0.5,\ 1/\sqrt{2},\ 1.0$.

III. BERRY CURVATURE OF COUPLED WAVES BETWEEN MAGNONS AND ELECTROMAGNETIC WAVES FOR THE CASE WITH $\theta = \pi/2$ ($k_z = 0$)

When $\boldsymbol{k}$ is perpendicular to the magnetization M_0 ($\theta = \pi/2$), the wave vector becomes the two-dimensional vector, $\boldsymbol{k} = (k_x, k_y) = k(\cos\varphi, \sin\varphi)$, and Eq. (18) reduces to

$$\left[\omega^4 - \left(\omega_{em}^2 + \omega_s^2\right)\omega^2 + \omega_{em}^2\omega_s\omega_H\right]\left[\omega^2 - \omega_{em}^2\right] = 0. \quad (19)$$

The eigenfrequencies from the first and second parentheses correspond to the set of components m_x, m_y, b_x, b_y, e_z, and that of b_z, e_x, e_y, respectively. The decoupling between these two sets is due to a mirror symmetry with respect to the xy plane, under which the wave vector $\boldsymbol{k}$ is invariant for the case with $\theta = \pi/2$. The eigenmodes for m_x, m_y, b_x, b_y, and e_z are odd under mirror symmetry, corresponding to TE modes, whereas the eigenmode for b_z, e_x, e_y is even under mirror symmetry, corresponding to a TM mode. The first set comprises the hybrid waves of a magnon and an electromagnetic wave,

$$\omega_\pm^2 = \frac{\omega_s^2 + \omega_{em}^2}{2} \pm \sqrt{\left(\frac{\omega_s^2 - \omega_{em}^2}{2}\right)^2 + (\zeta k)^2}. \quad (20)$$

Meanwhile within the linearized EOM, the second set of the fields (b_z, e_x, e_y) represents a pure electromagnetic wave and is free from the hybridization with magnon with its frequency equal to ω_{em}, satisfying $\omega_- < \omega_{em} < \omega_+$ [Figs. 2(a) and 3(a)]. Here

$$\zeta \equiv \sqrt{\frac{\omega_M\omega_s}{\epsilon}}c \quad (21)$$

stands for the hybridization strength between magnon and electromagnetic waves. For the ω_+ branch of Eq. (20), the dispersion at $k \to \infty$ and $k \to 0$ has the following asymptotic forms,

$$\omega_+^2 \simeq \begin{cases} \omega_{em}^2 + \frac{(\zeta k)^2}{\omega_{em}^2} & (k \to \infty), \\ \omega_s^2 + \frac{(\zeta k)^2}{\omega_s^2} & (k \to 0), \end{cases} \quad (22)$$

and for the ω_- branch of Eq. (20) is

$$\omega_-^2 \simeq \begin{cases} \omega_s^2 - \frac{(\zeta k)^2}{\omega_{em}^2} = \omega_{\rm mag}^2 & (k \to \infty), \\ \omega_{em}^2 - \frac{(\zeta k)^2}{\omega_s^2} & (k \to 0), \end{cases} \quad (23)$$

where $\omega_{\rm mag}^2 = \omega_H\omega_s = \omega_H(\omega_H + \omega_M)$ is the dispersion of the magnon in the magnetostatic regime. At the $k = 0$ limit, the magnon at $\omega = \omega_s$ and the electromagnetic waves become decoupled, as can be seen in the equations of motion. Therefore, the electromagnetic wave with $\omega = \omega_-$ remains gapless even in the presence of its coupling with the magnon.

Let k^* and $\tilde{\omega}$ denote the wave number and frequency at a crossing point between the dispersions of the magnon ω_s and the electromagnetic wave ω_{em} without the coupling ($\zeta = 0$);

$$\omega_s = \omega_{em}(k^*) \equiv \tilde{\omega}, \quad k^* \equiv \frac{\sqrt{\epsilon}\omega_s}{c}. \quad (24)$$

The frequencies of the coupled wave at the crossing point $k = k^*$ is given by

$$\omega_\pm = \sqrt{\tilde{\omega}^2 \pm \tilde{\omega}\Delta\omega}, \quad \Delta\omega \equiv \frac{\zeta k^*}{\tilde{\omega}}, \quad (25)$$

where $\Delta\omega$ is defined as a hybridization gap at the crossing point. Note that the crossing point is located outside the magnetostatic regime. By using Eqs. (3)–(4), the magnetic field and the magnetization are written as [37]

$$\boldsymbol{h_k} = \frac{4\pi}{1 - \omega^2/\omega_{em}^2}\left(-\frac{\boldsymbol{k}\cdot\boldsymbol{m_k}}{k^2}\boldsymbol{k} + \frac{\omega^2}{\omega_{em}^2}\boldsymbol{m_k}\right), \quad (26)$$

$$\boldsymbol{k}\times\boldsymbol{h_k} = \frac{\omega^2/\omega_{em}^2}{1 - \omega^2/\omega_{em}^2}\boldsymbol{k}\times\boldsymbol{m_k}. \quad (27)$$

The magnetostatic regime is defined by $\omega \ll \omega_{em}$, where the magnetic field becomes approximately rotation free, $\boldsymbol{h}_{\boldsymbol{k}} \simeq -4\pi(\boldsymbol{k}\cdot\boldsymbol{m}_{\boldsymbol{k}})\boldsymbol{k}/k^2$ and $\boldsymbol{k}\times\boldsymbol{h}_{\boldsymbol{k}} \simeq \boldsymbol{0}$. It is obvious that the crossing point ($\omega \simeq \omega_{em}$) sits far outside the magnetostatic regime. In the following, we will show that the Berry curvature of the coupled modes shows a prominent peak near the crossing point outside the magnetostatic regime.

The coupled modes between magnons and electromagnetic waves involve the components m_x, m_y, b_x, b_y, and e_z. The eigenvalue equation for the coupled modes is given by a 5×5 matrix extracted from $\tilde{H}_{\rm eff}$:

$$\tilde{H}^{\perp}_{\rm eff}(\boldsymbol{k})\boldsymbol{x}_{\boldsymbol{k},\pm} = \omega_{\pm}\gamma^{\perp}\boldsymbol{x}_{\boldsymbol{k},\pm}, \tag{28}$$

with

$$\tilde{H}^{\perp}_{\rm eff}(\boldsymbol{k}) = \begin{pmatrix} 0 & -i\frac{(4\pi)^2\omega_s^2}{\omega_M} & 0 & 4\pi i\omega_s & -4\pi ck_y \\ i\frac{(4\pi)^2\omega_s^2}{\omega_M} & 0 & -4\pi i\omega_s & 0 & 4\pi ck_x \\ 0 & 4\pi i\omega_s & 0 & -i\omega_M & ck_y \\ -4\pi i\omega_s & 0 & i\omega_M & 0 & -ck_x \\ -4\pi ck_y & 4\pi ck_x & ck_y & -ck_x & 0 \end{pmatrix}. \tag{29}$$

The energy density of the hybridized modes is given by a norm of a five-components eigenvector, $\boldsymbol{x}_{\boldsymbol{k}} \equiv {}^t(m_{\boldsymbol{k},x}, m_{\boldsymbol{k},y}, b_{\boldsymbol{k},x}, b_{\boldsymbol{k},y}, e_{\boldsymbol{k},z})$. The norm is given by $\boldsymbol{x}^{\dagger}_{\boldsymbol{k}}\gamma^{\perp}\boldsymbol{x}_{\boldsymbol{k}}$, where $\gamma^{\perp}$ is a 5×5 hermitian matrix extracted from the matrix γ: with

$$\gamma^{\perp} \equiv \begin{pmatrix} \frac{(4\pi)^2\omega_s}{\omega_M} & 0 & -4\pi & 0 & 0 \\ 0 & \frac{(4\pi)^2\omega_s}{\omega_M} & 0 & -4\pi & 0 \\ -4\pi & 0 & 1 & 0 & 0 \\ 0 & -4\pi & 0 & 1 & 0 \\ 0 & 0 & 0 & 0 & \epsilon \end{pmatrix}. \tag{30}$$

Based on this normalization, the Berry curvature of the coupled modes for the $\omega_{\pm}$ branches is defined as

$$\Omega_{z,n}(\boldsymbol{k}) = i\epsilon_{\alpha\beta}\frac{\partial \boldsymbol{x}^{\dagger}_{\boldsymbol{k},n}}{\partial k_{\alpha}}\gamma^{\perp}\frac{\partial \boldsymbol{x}_{\boldsymbol{k},n}}{\partial k_{\beta}} \tag{31}$$

for $n=\pm$, $\boldsymbol{k}=(k_x,k_y)=k(\cos\varphi,\sin\varphi)$, and $\alpha,\beta=x,y$ with $\boldsymbol{x}^{\dagger}_{\boldsymbol{k},n}\gamma^{\perp}\boldsymbol{x}_{\boldsymbol{k},n}=1$. Here $\epsilon_{\alpha\beta}$ is the antisymmetric tensor with $\epsilon_{xy}=-\epsilon_{yx}=1$. After a lengthy calculation, we find that the Berry curvature depends only on k;

$$\Omega_{z,\pm}(k) = \frac{1}{k}\frac{\partial}{\partial k}\left(\frac{\frac{\omega_{\pm}}{\omega_s}\left(\omega_{\pm}^2-\omega_{em}^2\right)}{\left(2\omega_{\pm}^2-\omega_s^2-\omega_{em}^2\right)}\right). \tag{32}$$

The details of the derivation are shown in Appendix B. By the similar procedure as in the magnetoelastic wave [35], we henceforth calculate the Berry curvature in the regimes with weak and strong coupling defined by $\Delta\omega/\tilde{\omega} \ll 1$ and $\Delta\omega/\tilde{\omega} \simeq 1$, respectively.

A. Weak coupling regime

The weak-coupling regime between magnon and electromagnetic wave is expressed as $\omega_M \ll \omega_s$ from Eqs. (21), (24), and (25). To satisfy this condition, we set $\omega_M \ll \omega_H$ to calculate the Berry curvature. When $\omega_M \ll \omega_H$, the hybridization gap is approximately evaluate as

$$\Delta\omega \simeq \sqrt{\omega_M\omega_H}. \tag{33}$$

The gap is much smaller than $\tilde{\omega}$ under this condition. We show the results of the numerical calculation of the dispersion and the Berry curvature in Figs. 2(a) and 2(b). The Berry curvatures for $\omega_{\pm}$ show a strong peak and are localized at the crossing point of the dispersions.

The peak value of the Berry curvature at the crossing point ($k=k^*$) is approximately evaluated as

$$\Omega_{z,\pm}(k=k^*) = \mp\frac{\tilde{\omega}^2}{2k^{*3}\zeta} = \mp\frac{1}{2k^{*2}\Delta\omega/\tilde{\omega}}. \tag{34}$$

In terms of $\tilde{\omega}\simeq\omega_H$, and $\Delta\omega\simeq\sqrt{\omega_M\omega_H}$, we can see that the Berry curvature is proportional to $\Omega_{\pm}(k^*)\propto 1/\omega_M^{1/2}$ and $1/\omega_H^{3/2}$. The dependences of the Berry curvature on ω_M and ω_H agree with Figs. 2(c) and 2(d). This result has the same form as the result of the magnetoelastic wave with respect to the hybridization gap except for some coefficients [35]. It means that the main effect of the Berry curvature induced by the hybridization has a universal feature around the hybridization gap in the weak coupling regime.

B. Strong coupling regime

To calculate the Berry curvature in the strong-coupling regime, we set $\omega_M \simeq \omega_s$. The results of the dispersion and the Berry curvature are shown in Fig. 3. When the coupling between magnon and electromagnetic wave is strong, the peak of the Berry curvature at $k=k^*$ broadens as shown in Figs. 3(a) and 3(b).

The Berry curvature of the coupled wave is affected by the hybridization even at $k \ll k^*$. By using Eq. (32) and the dispersions Eqs. (22) and (23), we obtain the Berry curvature for $k \ll k^*$

$$\Omega_{z,+}(k) \sim -\frac{\zeta^2}{\omega_s^4}, \tag{35}$$

$$\Omega_{z,-}(k) \sim \frac{3\zeta^2 c' k}{\omega_s^5}, \tag{36}$$

where $c'=\sqrt{c^2/\epsilon-\zeta^2/\omega_s^2}$. These results show that the Berry curvature for $k\ll k^*$ is strongly affected by the coupling ζ. The Berry curvature $\Omega_{z,+}$ is finite at $k\to 0$, while the Berry curvature $\Omega_{z,-}$ is zero at $k\to 0$. The analytical results agree with the result of Figs. 3(c) and 3(d).

The asymptotic behavior of $\Omega_{z,-}$ around $k\simeq 0$ comes from the linearly polarized nature of the magnetic field and flux in the vicinity of $k=0$. For simplicity, we choose the wave vector $\boldsymbol{k}=k\boldsymbol{e}_y$ where $\boldsymbol{e}_y$ is a unit vector along the y axis. A relation between h_x and h_y is written for the ω_{em} mode as [37]

$$\frac{h_y}{h_x} = -\frac{i\omega\omega_M}{\omega_{\rm mag}^2-\omega^2}. \tag{37}$$

Thus, the magnetic field becomes linearly polarized along the x direction when $k\to 0$. In addition, the magnetic flux also becomes linearly polarized along x at $k\to 0$, because the nondiagonal component of the permeability tensor μ_{xy} becomes smaller at $k\to 0$. These behaviors are the same for

an arbitrary direction of $\boldsymbol{k}$. Thus, the eigenvector becomes asymptotically independent of k and the Berry curvature $\Omega_{z,-}(k)$ becomes zero at $k \to 0$. This asymptotic behavior of the Berry curvature for the $\omega = \omega_-$ mode is totally different from that of the magnetoelastic wave $\omega = \omega_+$ in the strong coupling, where the Berry curvature of the linearly dispersive branch diverges toward $k = 0$.

IV. TOPOLOGICAL EDGE MODES AT $k_z = 0$

A. Chern number

Let us define an integral of the Berry curvature for the ω_n branch over the two-dimensional momentum space [41,42];

$$\mathrm{Ch}_n = \int_{-\infty}^{+\infty}\int_{-\infty}^{+\infty} \Omega_{z,n}(\boldsymbol{k})\frac{dk_x dk_y}{2\pi}, \tag{38}$$

with $n = \pm$. The integral is quantized to be an integer (Chern number), when the ω_n branch is separated from the other branches by a direct gap for any $\boldsymbol{k} = (k_x, k_y)$. The quantized integer is identical with a number of topological chiral edge modes inside the gap [43]. The edge modes are localized along a boundary of the system within the xy plane. Using Eq. (32), we obtain

$$\begin{aligned}\mathrm{Ch}_n &= \int_0^{\infty} dk \frac{\partial}{\partial k}\left(\frac{\frac{\omega_n}{\omega_s}\left(\omega_n^2 - \omega_{em}^2\right)}{\left(2\omega_n^2 - \omega_s^2 - \omega_{em}^2\right)}\right) \\ &= N_n(\infty) - N_n(0),\end{aligned} \tag{39}$$

where

$$N_n(k_0) \equiv \left(\frac{\frac{\omega_n}{\omega_s}\left(\omega_n^2 - \omega_{em}^2\right)}{\left(2\omega_n^2 - \omega_s^2 - \omega_{em}^2\right)}\right)\Bigg|_{k\to k_0}. \tag{40}$$

Using Eqs. (22) and (23), we have

$$N_+(k) = \begin{cases} 0 & (k \to \infty) \\ 1 & (k \to 0) \end{cases}, \tag{41}$$

and

$$N_-(k) = \begin{cases} \frac{\omega_{\mathrm{mag}}}{\omega_s} & (k \to \infty) \\ 0 & (k \to 0) \end{cases}. \tag{42}$$

Thus, the Chern number for the ω_+ branch is -1,

$$\mathrm{Ch}_+ = -1. \tag{43}$$

The dispersion and its Chern number are illustrated in Fig. 4(a). From the quantization of the Chern number, we expect that a chiral edge mode with $k_z = 0$ appears inside the hybridization gap between the ω_+ branch and ω_- branch.

The integral of the Berry curvature for the ω_- branch is not quantized to an integer. This is because the ω_- branch in the particle space ($\omega = \omega_- \geqslant 0$) and its hole counterpart ($\omega = -\omega_- \leqslant 0$) forms a band touching at $k = 0$; $\omega_-(k = 0) = 0$. In the eigenvalue equation (6), the branch with the positive frequency and that with the negative frequency are coupled with each other. Due to the band touching at $k = 0$, the Chern number for the ω_- branch is not well defined. As a result, the sum of the Chern number over the branches with the positive frequency region is not zero either, unlike the cases with a gap between the positive ω and the negative ω branches [26].

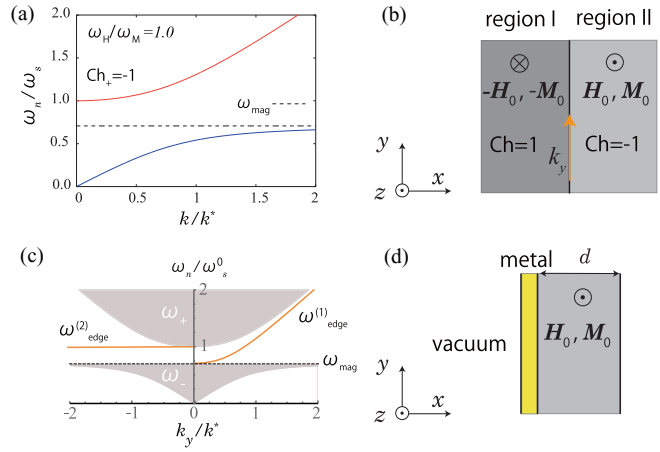

FIG. 4. Topological Chern number and topological edge modes of coupled waves between magnons and electromagnetic waves. (a) Dispersions of the ω_+ and ω_- branches with the Chern number for the ω_+ branch. (b) Schematic picture of two ferromagnetic regions with opposite magnetization and magnetic field. In region I, the Chern number of the ω_+ branch is $+1$ with $\boldsymbol{H} = (0, 0, -H_0)$, and in region II it is -1 with $\boldsymbol{H} = (0, 0, H_0)$. The boundary between the two regions is parallel to the y axis. We define the surface momentum along y as k_y. (c) Dispersions for the edge modes (orange lines) with $\omega_H^0 = \omega_M^0 = 5.0$ (GHz). Gray-colored regions show projections of the dispersions of the bulk modes ω_+ and ω_- onto the surface momentum k_y. (d) Ferromagnetic insulator slab with a metalized surface. A chiral mode appears only in the $k_y < 0$ on the metalized surface.

B. Chiral edge modes

From the quantization of the Chern number of the ω_+ branch, we expect that a chiral edge mode with $k_z = 0$ appears inside the hybridization gap. The mode is localized at a boundary between topologically different regions. Here, we show an emergence of such topological chiral edge modes at an interface between two regions with opposite magnetizations. We consider a domain wall as schematically illustrated in Fig. 4(b). The magnetization and magnetic field is directed along $-z$ direction in region I ($x < 0$) and $+z$ direction in region II ($x > 0$). Namely, $\boldsymbol{H} = (0, 0, H_0)$, $\boldsymbol{M} = (0, 0, M_0)$ in region II and $\boldsymbol{H} = (0, 0, -H_0)$, $\boldsymbol{M} = (0, 0, -M_0)$ in region I, where H_0 and M_0 are positive. This means $\omega_H = \omega_H^0 \equiv gH_0$, $\omega_M = \omega_M^0 \equiv 4\pi gM_0$, and $\omega_s = \omega_s^0 \equiv \omega_H^0 + \omega_M^0$ in region II and $\omega_H = -\omega_H^0$, $\omega_M = -\omega_M^0$, and $\omega_s = -\omega_s^0$ in region I. From Eq. (32), the Berry curvature for the ω_n branch changes its sign from region I to region II. Thus, the Chern number for the ω_+ branch in region I is $+1$, while that in region II is -1.

The number of chiral edge modes at an interface with two regions with different Chern numbers equals to the difference of the two Chern numbers between the two regions [43]. It is independent of the details of the interface. Since the Chern number in region I and in region II are 1 and -1, respectively, two chiral edge modes are expected to emerge at the interface. To see them, we note that the wave number k_y along the edge (y axis) is conserved, while we should replace k_x by $-i\partial_x$ in Eq. (29). We then calculate eigenmodes of Eq. (28) at the boundary. The eigenmodes localized at the boundary is proportional to $e^{ik_y y + \kappa x}$ for $x < 0$ and $e^{ik_y y - \kappa x}$ for $x > 0$ with $\kappa > 0$. From

the boundary conditions for the electromagnetic waves b_x, h_y, and e_z, we obtain two edge-mode solutions $\omega = \omega^{(1)}_{\rm edge}$, $\omega^{(2)}_{\rm edge}$ inside the gap between ω_+ and ω_- (see Appendix E), and their dispersion relations are shown in Fig. 4(c). The dispersions of the edge modes are written as

$$\left(\omega^{(1)}_{\rm edge}\right)^2 = \frac{\omega^2_{\rm mag}+\omega^2_{em}}{2} + \sqrt{\left(\frac{\omega^2_{\rm mag}+\omega^2_{em}}{2}\right)^2 - \omega_H^2\omega^2_{em}} \quad (k_y > 0), \tag{44}$$

$$\omega^{(2)}_{\rm edge} = \omega^0_s \quad (k_y < 0), \tag{45}$$

with $\omega_{em} = ck_y/\sqrt{\epsilon}$ and $k_y > 0$. The dispersion $\omega^{(1)}_{\rm edge}$ touches at $k_y = 0$ the top of the ω_- branch of the bulk mode. The dispersion quadratically increases in small k_y for $k_y \sim k^*$ due to the magnon, while it linearly increases for $k_y \gg k^*$ because the electromagnetic wave is dominant. The other edge mode $\omega^{(2)}_{\rm edge}$ shows a flat dispersion as in Fig. 4(c) with $k_y < 0$.

An edge mode with a flat dispersion similar to Eq. (45) was also reported in a previous study of topological edge magnetoplasmon [27]. The magnetoplasmon is a coupled wave between the charge density and electric current density in a two-dimensional electron gas (2DEG) under a high magnetic field. The previous study [27] found two distinct edge modes in the 2DEG under the magnetic field, one edge mode with a flat dispersion and the other edge mode with a linear (chiral) dispersion. The edge mode with the flat dispersion carries only the electric current component, while the other edge mode carries both charge density and current components. Similarly to the topological magnetoedgeplasmon, the edge mode with the flat dispersion in the present system, Eq. (45), carries only the magnetization and the magnetic field components but not the electric field component (see Appendix E). Meanwhile, the edge mode with the chiral dispersion, Eq. (44), is a coupled mode among magnetization, magnetic field, and electric field (see Appendix E1).

The edge mode with the flat dispersion in Eq. (45) can be regarded as the Damon-Eshbach surface mode in a ferromagnetic insulator slab with its surface being metalized [44]. A dispersion of the surface mode of the surface-metalized ferromagnetic insulator slab with a finite thickness d exists only in the $k_y < 0$ region in Fig. 4(d). When the thickness becomes much larger than the wavelength ($|k_y d| \gg 1$), the dispersion becomes flat when the exchange interaction is neglected [44] and the saturated dispersion equals to Eq. (45). Note also that the boundary condition for the magnetic flux in the edge mode with the flat dispersion $\omega = \omega^0_s$ (see Appendix E) is the same as that in the surface-metalized ferromagnet, where the magnetic flux density along the x direction at the surface is zero due to the metalized surface [44].

C. Discussion

In this section, we first discuss the case with $\theta \neq 0$ (k_z is nonzero). The Chern number is defined only when the bands are separated by a full gap for the entire $\boldsymbol{k}$ space within the k_x-k_y plane. When $\theta = \pi/2$ ($k_z = 0$), electromagnetic waves are classified into TE and TM modes by their properties under the mirror symmetry. Only the TE mode is coupled with the magnon in this situation. There is always a gap between the magnon and the TE mode, and the Chern number can be defined as explained above. When $\theta \neq 0$ (k_z is nonzero), the two modes of electromagnetic waves are coupled with the magnon, and there is no full gap. Therefore, the Chern number cannot be defined, and topological edge modes do not exist in a strict sense.

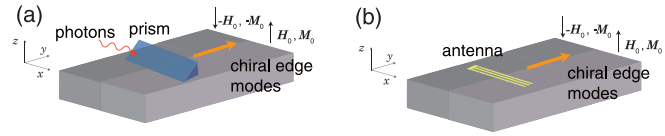

FIG. 5. Schematic illustration of excitations of chiral edge modes by (a) injecting electromagnetic waves (photons) and (b) injecting magnons via an antenna.

Next, we discuss how to detect the chiral edge modes in experiments. We only focus on the dispersive chiral edge mode, namely the coupled wave between the magnon and the electromagnetic wave. There are generally two methods of generating chiral edge modes into a magnetic material: one is by injecting electromagnetic waves [45–47] and the other is by exciting magnons via an antenna. These two methods are shown schematically in Figs. 5(a) and 5(b), respectively. In the former method, electromagnetic waves can be injected into the ferromagnet directly when the edge mode considered is inside the light cone ($\omega > ck/\sqrt{\epsilon}$). On the other hand, when the edge mode is outside the light cone ($\omega < ck/\sqrt{\epsilon}$), we need to use a particular method to inject the electromagnetic wave into the ferromagnet. For example, we can use a prism similar to the Kretschmann configuration, used for exciting surface plasmon modes. Electromagnetic waves are injected along the domain wall through the prism and hybridized with the magnons to generate a chiral edge mode. Then the chiral edge mode can either be measured as a magnon by several methods for magnon detection (such as Brillouin light scattering) or as an electromagnetic wave via the same methods as the injection. The predicted chiral nature can be verified by changing the injection and observation points on the edges in the experimental setup.

As mentioned above, chiral edge modes are defined only for $k_z = 0$ because of the separation between the TE and TM modes. When k_z is nonzero, topological edge modes do not appear because the Chern number is not defined. However, the edge modes do not disappear immediately when k_z is changed from zero to nonzero. The edge modes will remain as a transient mode, which gradually leaks into the bulk modes. This leakage will be prominent when k_z is away from zero.

V. CONCLUSION

In this paper, we discuss the Berry curvature and topological edge modes that emerge from a hybridization between a magnon and an electromagnetic wave in a ferromagnetic insulator. By introducing a norm of eigenvector for the coupled wave based on the energy conservation, we reformulated the Landau-Lifshitz-Maxwell equation into a Hermitian eigenvalue equation. From the eigenvalue equation, we introduced the Berry curvature of the coupled waves between the magnon and the electromagnetic wave. When the wave vector of the

coupled wave $\boldsymbol{k}$ is perpendicular to the magnetic field and magnetization, we found that the Berry curvature shows a prominent peak around a hybridization point between the magnon and the electromagnetic modes. The hybridization leads to two relevant hybrid modes; one is a magnonlike massive mode ($\omega = \omega_+$) at $\boldsymbol{k} = 0$ and the other is a photonlike massless mode ($\omega = \omega_-$) at $\boldsymbol{k} = 0$. Around $\boldsymbol{k} \simeq 0$, the Berry curvature for the massless mode converges to zero, while that for the massive mode converges to a nonzero value. We found that the Chern number for the massive mode takes a nonzero integer (± 1), and consequently two chiral edge modes emerge inside the hybridization gap at a domain wall between two ferromagnetic insulators with opposite magnetizations. One of the two edge modes carries both a magnon and an electromagnetic wave, while the other edge mode is purely magnetic and can be regarded as the Damon-Eschbach surface chiral mode of the surface-metalized ferromagnetic insulator slab.

Recently, the surface mode of the ferromagnet film in the dipole-exchange regime immune to backscattering is reported [48]. Our work provides an insight for the search of the chiral edge modes and stimulates future simulational and experimental studies on coupled waves between magnons and electromagnetic waves.

ACKNOWLEDGMENTS

This work was supported by a Ministry of Education, Culture, Sports, Science, and Technology (MEXT) KAKENHI Grant No. JP26100006 and by Japan Science and Technology Agency (JST) CREST Grant No. JPMJCR14F1. R.S. was supported by the National Basic Research Programs (NBRP) of China (973 program, with the Grants No. 2014CB92090 and No. 2015CB921104) and the National Natural Science Foundation of China (Grant No. is 11674011).

APPENDIX A: DERIVATION OF THE EQUATIONS OF MOTION FOR THE COUPLED WAVE BETWEEN THE MAGNON AND THE ELECTROMAGNETIC WAVE

In this Appendix, we derive dynamical equations of motion of magnons and electromagnetic waves with an arbitrary angle between the saturation magnetization and the wave vector in a ferromagnetic insulator. We assume the saturation magnetization $\boldsymbol{M}_0$ and the applied magnetic field $\boldsymbol{H}_0$ are along the z direction. The magnon is represented as a small vector $\boldsymbol{m}$ in the xy plane: $\boldsymbol{M} = \boldsymbol{m} + M_0\boldsymbol{e}_z$. So does the magnetic field $\boldsymbol{H}$ as $\boldsymbol{H} = \boldsymbol{h} + H_0\boldsymbol{e}_z$, where $\boldsymbol{h}$ is a small magnetic field ($|\boldsymbol{h}| \ll H_0$). The system is dielectrically isotropic and an energy dissipation is neglected. We consider only Zeeman interaction and fluctuation of the magnetic field oscillation as fields acting onto magnons. We neglect an exchange interaction because the wave number at the crossing between the magnon and the electromagnetic waves is typically much smaller than an inverse of a lattice constant of crystalline magnetic material. The effective field $\boldsymbol{H}_{\rm eff}$ is written as

$$\boldsymbol{H}_{\rm eff} = \boldsymbol{h} - \frac{H_0}{M_0}\boldsymbol{m}. \tag{A1}$$

The equation of motion for magnons are given by the Landau-Lifshitz equation:

$$\frac{\partial \boldsymbol{M}}{\partial t} = -g\boldsymbol{M} \times \boldsymbol{H}_{\rm eff}, \tag{A2}$$

where g is the gyromagnetic ratio. The electromagnetic fields are determined by the Maxwell equation:

$$\frac{\partial \boldsymbol{b}}{\partial t} = -c\nabla \times \boldsymbol{e}, \tag{A3}$$

$$\epsilon \frac{\partial \boldsymbol{e}}{\partial t} = c\nabla \times \boldsymbol{h}, \tag{A4}$$

where c is the speed of light. Assuming the magnetization $\boldsymbol{m}$, and the electromagnetic fields $\boldsymbol{h}$ and $\boldsymbol{e}$ are proportional to $\exp(i\boldsymbol{k}\cdot\boldsymbol{x})$, where $\boldsymbol{k}$ is a wave vector, and expanding Eq. (A2) to the linear order in $\boldsymbol{h}$ and $\boldsymbol{m}$, we obtain Eqs. (1)–(4) with $\boldsymbol{b} = \boldsymbol{h} + 4\pi\boldsymbol{m}$.

In Sec. III, we calculate the dispersion relation where the wave vector is perpendicular to the magnetization. In this Appendix A, we consider the case with $\boldsymbol{k} \parallel \boldsymbol{M}_0$. From Eq. (18), the dispersion relation reduces to

$$\left[\omega\left(\omega^2 - \omega_{em}^2\right) - \left(\omega_s\omega^2 - \omega_H\omega_{em}^2\right)\right] \times \left[\omega\left(\omega^2 - \omega_{em}^2\right) + \omega_s\omega^2 - \omega_H\omega_{em}^2\right] = 0. \tag{A5}$$

From this, we obtain the dispersion relations for three branches shown in Ref. [37]. Let ω_i ($i = 1, 2, 3$) be the eigenfrequencies of the waves with $0 < \omega_1 < \omega_2 < \omega_3$. Among the three modes with positive frequencies, one is massive at $k = 0$, $\omega(k = 0) \neq 0$, while the other two are massless at $k = 0$. The dispersions of the massless modes take the following asymptotic forms around $k = 0$,

$$\omega_1 \approx \omega_{em}\sqrt{\frac{\omega_H}{\omega_s}} - \frac{\omega_M\omega_{em}^2}{2\omega_s^2}, \tag{A6}$$

and

$$\omega_2 \approx \omega_{em}\sqrt{\frac{\omega_H}{\omega_s}} + \frac{\omega_M\omega_{em}^2}{2\omega_s^2}. \tag{A7}$$

The dispersion of the massive mode has the following asymptotic form near $k = 0$,

$$\omega_3 \approx \omega_s + \frac{\omega_M\omega_{em}^2}{\omega_s^2}. \tag{A8}$$

APPENDIX B: CALCULATION OF THE BERRY CURVATURE OF THE COUPLED WAVE BETWEEN THE MAGNON AND THE ELECTROMAGNETIC WAVE

In this Appendix, we give a detailed calculation of the Berry curvature for the coupled modes between a magnon and an electromagnetic wave for the case with $\boldsymbol{k} \perp \boldsymbol{M}_0$. Let $\boldsymbol{M}_0$ to be along the z axis. The two relevant branches with $\omega = \omega_\pm$ represent hybridized waves of m_x, m_y, b_x, b_y, and e_z. The eigenvalue equation for these five components, $\boldsymbol{x}_{\boldsymbol{k}} \equiv {}^t(m_{\boldsymbol{k},x}, m_{\boldsymbol{k},y}, b_{\boldsymbol{k},x}, b_{\boldsymbol{k},y}, e_{\boldsymbol{k},z})$, is given by:

$$\tilde{H}_{\rm eff}^{\perp}(k, \varphi)\boldsymbol{x}_{\boldsymbol{k}} = \omega\gamma^{\perp}\boldsymbol{x}_{\boldsymbol{k}}, \tag{B1}$$

where

$$\tilde{H}^{\perp}_{\rm eff}(k,\varphi)=\gamma^{\perp}H_{\rm eff}(k,\varphi)=\begin{pmatrix} 0 & -i\frac{(4\pi)^2\omega_s^2}{\omega_M} & 0 & 4\pi i\omega_s & -4\pi ck_y \\ i\frac{(4\pi)^2\omega_s^2}{\omega_M} & 0 & -4\pi i\omega_s & 0 & 4\pi ck_x \\ 0 & 4\pi i\omega_s & 0 & -i\omega_M & ck_y \\ -4\pi i\omega_s & 0 & i\omega_M & 0 & -ck_x \\ -4\pi ck_y & 4\pi ck_x & ck_y & -ck_x & 0 \end{pmatrix}. \tag{B2}$$

Here $\boldsymbol{k}\equiv k(\cos\varphi,\ \sin\varphi)$ is within the xy plane, with φ being the angle between the x axis (see Fig. 1). The norm of the eigenvector is defined through the Hermitian matrix $\gamma^{\perp}$;

$$\gamma^{\perp}=\begin{pmatrix} \frac{(4\pi)^2\omega_s}{\omega_M} & 0 & -4\pi & 0 & 0 \\ 0 & \frac{(4\pi)^2\omega_s}{\omega_M} & 0 & -4\pi & 0 \\ -4\pi & 0 & 1 & 0 & 0 \\ 0 & -4\pi & 0 & 1 & 0 \\ 0 & 0 & 0 & 0 & \epsilon \end{pmatrix}. \tag{B3}$$

From the O(2) rotational symmetry in the Landau-Lifshitz-Maxwell equation, the eigenvector at finite φ is related to that at $\varphi=0$ by the O(2) transformation,

$$\tilde{H}^{\perp}_{\rm eff}(k,\varphi=0)\tilde{\boldsymbol{x}}_k=\omega\gamma^{\perp}\tilde{\boldsymbol{x}}_k, \tag{B4}$$

$$\boldsymbol{x_k}=\begin{pmatrix} \boldsymbol{U}_2(\varphi) & & \\ & \boldsymbol{U}_2(\varphi) & \\ & & 1 \end{pmatrix}\tilde{\boldsymbol{x}}_k, \tag{B5}$$

where

$$\boldsymbol{U}_2(\varphi)=\begin{pmatrix} \cos\varphi & -\sin\varphi \\ \sin\varphi & \cos\varphi \end{pmatrix}. \tag{B6}$$

The dependence on φ and k in $\boldsymbol{x_k}$ is now factorized into $\boldsymbol{U}_2(\varphi)$ and $\tilde{\boldsymbol{x}}_k$. $\tilde{\boldsymbol{x}}_k$ is an eigenstate of the following Hermitian matrix,

$$\tilde{H}^{\perp}_{\rm eff}(k,\varphi=0)=\begin{pmatrix} 0 & -i\frac{(4\pi)^2\omega_s^2}{\omega_M} & 0 & 4\pi i\omega_s & 0 \\ i\frac{(4\pi)^2\omega_s^2}{\omega_M} & 0 & -4\pi i\omega_s & 0 & 4\pi ck \\ 0 & 4\pi i\omega_s & 0 & -i\omega_M & 0 \\ -4\pi i\omega_s & 0 & i\omega_M & 0 & -ck \\ 0 & 4\pi ck & 0 & -ck & 0 \end{pmatrix}. \tag{B7}$$

By using the factorized form for $\boldsymbol{x_k}$, the Berry curvature is calculated as

$$\Omega_{z,n}(\boldsymbol{k})=i\epsilon_{\alpha\beta}\frac{\partial\boldsymbol{x}_{\boldsymbol{k}}^{\dagger}}{\partial k_\alpha}\gamma^{\perp}\frac{\partial\boldsymbol{x_k}}{\partial k_\beta}=\frac{1}{k}\frac{\partial}{\partial k}(\tilde{\boldsymbol{x}}_k^{\dagger}\Gamma\tilde{\boldsymbol{x}}_k), \tag{B8}$$

$$\Gamma=\begin{pmatrix} 0 & -\frac{(4\pi)^2\omega_s}{\omega_M} & 0 & 4\pi & 0 \\ \frac{(4\pi)^2\omega_s}{\omega_M} & 0 & -4\pi & 0 & 0 \\ 0 & 4\pi & 0 & -1 & 0 \\ -4\pi & 0 & 1 & 0 & 0 \\ 0 & 0 & 0 & 0 & 0 \end{pmatrix}, \tag{B9}$$

with the normalization condition $\tilde{\boldsymbol{x}}_k^{\dagger}\gamma^{\perp}\tilde{\boldsymbol{x}}_k=1$. To evaluate Eq. (B8), it is convenient to introduce an unnormalized eigenstate $\tilde{\boldsymbol{X}}_k$, which is related to $\tilde{\boldsymbol{x}}_k$ by

$$\tilde{\boldsymbol{x}}_k\equiv\frac{\tilde{\boldsymbol{X}}_k}{\sqrt{\tilde{\boldsymbol{X}}_k^{\dagger}\gamma^{\perp}\tilde{\boldsymbol{X}}_k}}. \tag{B10}$$

In terms of the unnormalized eigenstate, the Berry curvature is given by

$$\Omega_{z,n}(\boldsymbol{k})=\frac{1}{k}\frac{\partial}{\partial k}\left(\frac{\tilde{\boldsymbol{X}}_k\Gamma\tilde{\boldsymbol{X}}_k}{\tilde{\boldsymbol{X}}_k\gamma^{\perp}\tilde{\boldsymbol{X}}_k}\right). \tag{B11}$$

From the Hermitian eigenvalue equation, the eigenstate satisfies

$$\begin{pmatrix} -\frac{(4\pi)^2\omega_s\omega}{\omega_M} & -i\frac{(4\pi)^2\omega_s^2}{\omega_M} & 4\pi\omega & 4\pi i\omega_s & 0 \\ i\frac{(4\pi)^2\omega_s^2}{\omega_M} & -\frac{(4\pi)^2\omega_s\omega}{\omega_M} & -4\pi i\omega_s & 4\pi\omega & 4\pi ck \\ 4\pi\omega & 4\pi i\omega_s & -\omega & -i\omega_M & 0 \\ -4\pi i\omega_s & 4\pi\omega & i\omega_M & -\omega & -ck \\ 0 & 4\pi ck & 0 & -ck & -\epsilon\omega \end{pmatrix}\tilde{\boldsymbol{X}}_k=\boldsymbol{0}. \tag{B12}$$

Thus, we have

$$\tilde{\boldsymbol{X}}_k=\begin{pmatrix} -i\frac{\omega_M ck}{4\pi(\omega^2-\omega_s^2)} \\ \frac{\omega_s\omega_M ck}{4\pi\omega(\omega^2-\omega_s^2)} \\ 0 \\ -\frac{ck}{\omega} \\ 1 \end{pmatrix}. \tag{B13}$$

By using this wave function and Eq. (B11), we obtain the Berry curvature for the two eigenmodes with $\omega=\omega_{\pm}$:

$$\Omega_{z,\pm}(k)=\frac{1}{k}\frac{\partial}{\partial k}\left(\frac{\frac{\omega_{\pm}}{\omega_s}\left(\omega_{\pm}^2-\omega_{em}^2\right)}{\left(2\omega_{\pm}^2-\omega_s^2-\omega_{em}^2\right)}\right). \tag{B14}$$

APPENDIX C: WAVE NUMBER AND BERRY CURVATURE AT THE CROSSING POINT OF THE DISPERSIONS FOR THE ELECTROMAGNETIC WAVE AND THE MAGNON

Here we present a detailed calculation of the peak value of the Berry curvature at the crossing point between magnon and photon mode. The wave vector at the crossing point k^* is defined by

$$k^*=\sqrt{\frac{\epsilon}{c^2}}(\omega_H+\omega_M). \tag{C1}$$

The dispersion and the Berry curvature around $k = k^*$ are given by

$$\omega_\pm \simeq \sqrt{\frac{c^2(k^2+k^{*2})}{2\epsilon}} \times \left(1 \pm \frac{1}{(k^2+k^{*2})}\sqrt{\frac{(k^2-k^{*2})^2}{4} + \left(\frac{\epsilon\zeta k}{c^2}\right)^2}\right). \tag{C2}$$

Using Eqs. (B14) and (C2), we obtain peak values of the Berry curvature;

$$\Omega_{z,\pm}(k=k^*) = \mp\frac{\tilde{\omega}^2}{2k^{*3}\zeta} = \mp\frac{1}{2k^{*2}\Delta\omega/\tilde{\omega}}. \tag{C3}$$

APPENDIX D: HERMITIAN EIGENVALUE PROBLEMS IN THE OTHER BASES

In the main text, we use the basis for the eigenvector as $\boldsymbol{x}_{\boldsymbol{k},1} \equiv (\boldsymbol{m}_{\boldsymbol{k}}, \boldsymbol{b}_{\boldsymbol{k}}, \boldsymbol{e}_{\boldsymbol{k}})^t$. Using $\boldsymbol{b}_{\boldsymbol{k}} = \boldsymbol{h}_{\boldsymbol{k}} + 4\pi\boldsymbol{m}_{\boldsymbol{k}}$, one can change the basis for the eigenvector into either $\boldsymbol{x}_{\boldsymbol{k},2} \equiv (\boldsymbol{m}_{\boldsymbol{k}}, \boldsymbol{h}_{\boldsymbol{k}}, \boldsymbol{e}_{\boldsymbol{k}})^t$ or $\boldsymbol{x}_{\boldsymbol{k},3} \equiv (\boldsymbol{b}_{\boldsymbol{k}}, \boldsymbol{h}_{\boldsymbol{k}}, \boldsymbol{e}_{\boldsymbol{k}})^t$. In terms of $\boldsymbol{x}_{\boldsymbol{k},2}$, the Hermitian Hamiltonian in the eigenvalue problem changes into

$$H_2(\boldsymbol{k}) = \begin{pmatrix} 0 & -i\frac{(4\pi)^2\omega_H^2}{\omega_M} & 0 & 4\pi i\omega_H & 0 \\ i\frac{(4\pi)^2\omega_H^2}{\omega_M} & 0 & -4\pi i\omega_H & 0 & 0 \\ 0 & 4\pi i\omega_H & 0 & -i\omega_M & ck_y \\ -4\pi i\omega_H & 0 & i\omega_M & 0 & -ck_x \\ 0 & 0 & ck_y & -ck_x & 0 \end{pmatrix}. \tag{D1}$$

In the new basis, a norm of the eigenvectors should be redefined as $\langle \boldsymbol{x}_{\boldsymbol{k},2}|\gamma_2|\boldsymbol{x}_{\boldsymbol{k},2}\rangle$ with

$$\gamma_2 = \begin{pmatrix} \frac{(4\pi)^2\omega_H}{\omega_M} & 0 & 0 & 0 & 0 \\ 0 & \frac{(4\pi)^2\omega_H}{\omega_M} & 0 & 0 & 0 \\ 0 & 0 & 1 & 0 & 0 \\ 0 & 0 & 0 & 1 & 0 \\ 0 & 0 & 0 & 0 & \epsilon \end{pmatrix} \tag{D2}$$

(compare this with Eqs. (15), (16), and (17). We can also choose another basis, $\boldsymbol{x}_{\boldsymbol{k},3} \equiv (\boldsymbol{b}_{\boldsymbol{k}}, \boldsymbol{h}_{\boldsymbol{k}}, \boldsymbol{e}_{\boldsymbol{k}})^t$, with

$$H_3(\boldsymbol{k}) = \begin{pmatrix} 0 & -i\frac{\omega_H^2}{\omega_M} & 0 & i\frac{\omega_H\omega_s}{\omega_M} & 0 \\ i\frac{\omega_H^2}{\omega_M} & 0 & -i\frac{\omega_H\omega_s}{\omega_M} & 0 & 0 \\ 0 & i\frac{\omega_H\omega_s}{\omega_M} & 0 & -i\frac{\omega_s^2}{\omega_M} & ck_y \\ -i\frac{\omega_H\omega_s}{\omega_M} & 0 & i\frac{\omega_s^2}{\omega_M} & 0 & -ck_x \\ 0 & 0 & ck_y & -ck_x & 0 \end{pmatrix}, \tag{D3}$$

and

$$\gamma_3 = \begin{pmatrix} \frac{\omega_H}{\omega_M} & 0 & -\frac{\omega_H}{\omega_M} & 0 & 0 \\ 0 & \frac{\omega_H}{\omega_M} & 0 & -\frac{\omega_H}{\omega_M} & 0 \\ -\frac{\omega_H}{\omega_M} & 0 & \frac{\omega_s}{\omega_M} & 0 & 0 \\ 0 & -\frac{\omega_H}{\omega_M} & 0 & \frac{\omega_s}{\omega_M} & 0 \\ 0 & 0 & 0 & 0 & \epsilon \end{pmatrix}. \tag{D4}$$

The norm in this basis is defined as $\langle \boldsymbol{x}_{\boldsymbol{k},3}|\gamma_3|\boldsymbol{x}_{\boldsymbol{k},3}\rangle$. In accordance with the change of the norm, the Berry curvature in these new bases are defined by Eq. (31) with a replacement of $\gamma^\perp$ and $\boldsymbol{x}_{\boldsymbol{k}}$ by γ_2 and $\boldsymbol{x}_{\boldsymbol{k},2}$ or by γ_3 and $\boldsymbol{x}_{\boldsymbol{k},3}$, respectively. It is important to note that these different formulae give the same calculation result of the Berry curvature as Eq. (32).

APPENDIX E: CALCULATION OF THE EDGE-MODE SOLUTIONS OF THE COUPLED WAVE BETWEEN THE MAGNON AND THE ELECTROMAGNETIC WAVE

In the main text, we discuss the emergence of the chiral edge modes at the boundary between the two ferromagnetic regions with an opposite magnetization and magnetic field. In the following, we will give a detailed derivation of the edge modes and their dispersions. From Eq. (19) with the replacement of k_x by $\pm i\kappa$ ($\kappa > 0$), the eigenfrequencies of the edge modes should satisfy the following equation,

$$\omega^4 - \left(\tilde{\omega}_{em}^2 + \omega_s^2\right)\omega^2 + \tilde{\omega}_{em}^2\omega_{\rm mag}^2 = 0, \tag{E1}$$

$$\tilde{\omega}_{em}^2 \equiv \frac{c^2\left(k_y^2 - \kappa^2\right)}{\epsilon}. \tag{E2}$$

Unnormalized eigenvectors for the edge modes are obtained from Eqs. (B13) and (B5) with the replacement of k_x by $+i\kappa$ ($\kappa > 0$) for region II ($x > 0$) and by $-i\kappa$ for region I ($x < 0$); Eqs. (B13) and (B5) give the unnormalized eigenvectors at the both sides of the boundary,

$$\psi_{k_y}(x,y) = \begin{pmatrix} m_{x,k_y} \\ m_{y,k_y} \\ b_{x,k_y} \\ b_{y,k_y} \\ e_{z,k_y} \end{pmatrix} = C_\pm \begin{pmatrix} \pm\frac{\omega_M c\kappa}{4\pi} - \frac{\omega_s\omega_M ck_y}{4\pi\omega} \\ -i\frac{\omega_M ck_y}{4\pi} \pm i\frac{\omega_s\omega_M c\kappa}{4\pi\omega} \\ \frac{ck_y}{\omega}(\omega^2 - \omega_s^2) \\ \mp i\frac{c\kappa}{\omega}(\omega^2 - \omega_s^2) \\ (\omega^2 - \omega_s^2) \end{pmatrix} e^{\mp\kappa x + ik_y y}, \quad (x > 0\ (x < 0)) \tag{E3}$$

where $C_\pm$ are constants. Here, we note that $\omega_H = \omega_H^0 \equiv gH_0$, $\omega_M = \omega_M^0 \equiv 4\pi gM_0$, and $\omega_s = \omega_s^0 \equiv \omega_H^0 + \omega_M^0$ for $x > 0$ and $\omega_H = -\omega_H^0$, $\omega_M = -\omega_M^0$, and $\omega_s = -\omega_s^0$ for $x < 0$. Next, we need to determine the constant factors $C_\pm$ so as to satisfy the appropriate boundary conditions:

$$b_x(x=0+) = b_x(x=0-), \tag{E4}$$

$$e_z(x=0+) = e_z(x=0-), \tag{E5}$$

$$h_y(x=0+) = h_y(x=0-). \tag{E6}$$

In the following, to calculate edge-modes solutions, we study the case of $\omega \neq \omega_s^0$ and the case of $\omega = \omega_s^0$ separately.

1. Edge-mode solution with $\omega \neq \omega_s^0$

Let us first consider an edge-mode solution with $\omega \neq \omega_s^0$. From Eq. (E3), to satisfy the boundary conditions for b_x and e_z at $x = 0$ we need to set $C_+ = C_-$. Then the boundary condition for h_y at $x = 0$ gives a relation between κ and k_y,

$$\kappa = \frac{\omega_M^0\omega}{\omega^2 - \omega_{\rm mag}^2}k_y. \tag{E7}$$

A substitution of Eq. (E7) into Eqs. (E1) and (E2) leads to the dispersion relation between k_y and ω for localized modes:

$$\omega^4 - \left(\omega_{\rm mag}^2 + \omega_{em}^2\right)\omega^2 + \omega_H^2\omega_{em}^2 = 0, \tag{E8}$$

with $\omega_{em} \equiv ck_y/\sqrt{\epsilon}$ for $\omega \neq \omega_{\rm mag}$. It gives the chiral dispersion, Eq. (44), where $k_y > 0$ is required by the positiveness of κ.

The edge mode with the chiral dispersion involves both a magnetization and an electric field. For $k_y \to 0$, the chiral edge mode becomes magnonic,

$$\begin{pmatrix} m_{x,k_y}(x,y) \\ m_{y,k_y}(x,y) \\ b_{x,k_y}(x,y) \\ b_{y,k_y}(x,y) \\ e_{z,k_y}(x,y) \end{pmatrix} = C_\pm \begin{pmatrix} \frac{1}{4\pi\sqrt{2}}\sqrt{\frac{\omega_M}{\omega_s}} \\ \mp\frac{i}{4\pi\sqrt{2}}\sqrt{\frac{\omega_M}{\omega_H}} \\ 0 \\ \mp\frac{i}{\sqrt{2}}\sqrt{\frac{\omega_M}{\omega_H}} \\ 0 \end{pmatrix} e^{\mp\kappa x + ik_y y},$$
$$(x > 0\ (x < 0)). \tag{E9}$$

For $k_y \gg k^*$, the chiral mode becomes photonic,

$$\begin{pmatrix} m_{x,k_y}(x,y) \\ m_{y,k_y}(x,y) \\ b_{x,k_y}(x,y) \\ b_{y,k_y}(x,y) \\ e_{z,k_y}(x,y) \end{pmatrix} = C_\pm \begin{pmatrix} 0 \\ 0 \\ 1/\sqrt{2} \\ 0 \\ 1/\sqrt{2\epsilon} \end{pmatrix} e^{\mp\kappa x + ik_y y},$$
$$(x > 0\ (x < 0)). \tag{E10}$$

2. Edge-mode solution with $\omega = \omega_s^0$

First, Eq. (E3) satisfies the boundary conditions for b_x and e_z, while the boundary condition for h_y is satisfied by setting $C_- = -C_+$. Then, by combining $\omega = \omega_s^0$ with Eqs. (E1) and (E2), we relate k_y to κ as

$$\tilde{\omega}_{em}^2 \equiv \frac{c^2\left(k_y^2 - \kappa^2\right)}{\epsilon} = 0, \quad \Rightarrow k_y = \pm\kappa. \tag{E11}$$

A case with $k_y = +\kappa$ (> 0) makes all the components in Eq. (E3) be zero, giving no physical solution. The other case with $k_y = -\kappa\,(< 0)$ gives a physical edge-mode solution with the flat dispersion, Eq. (45). From Eq. (E3), the edge mode with the flat dispersion involves only the magnetization and the magnetic field;

$$\begin{pmatrix} m_{x,k_y}(x,y) \\ m_{y,k_y}(x,y) \\ b_{x,k_y}(x,y) \\ b_{y,k_y}(x,y) \\ e_{z,k_y}(x,y) \end{pmatrix} = C_\pm \begin{pmatrix} \pm\frac{1}{4\sqrt{2}\pi}\sqrt{\frac{\omega_M}{\omega_s}} \\ i\frac{1}{4\sqrt{2}\pi}\sqrt{\frac{\omega_M}{\omega_s}} \\ 0 \\ 0 \\ 0 \end{pmatrix} e^{\mp\kappa x + ik_y y},$$
$$(x > 0\ (x < 0)). \tag{E12}$$

[1] V. E. Demidov and B. A. Kalinikos, Tech. Phys. Lett. **26**, 729 (2000).
[2] V. E. Demidov, B. A. Kalinikos, and P. Edenhofer, J. Appl. Phys. **91**, 10007 (2002).
[3] V. E. Demidov, B. A. Kalinikos, and P. Edenhofer, Tech. Phys. **47**, 343 (2002).
[4] D. L. Mills and E. Burstein, Rep. Prog. Phys. **37**, 817 (1974).
[5] A. Lehmeyer and L. Merten, J. Magn. Magn. Mater. **50**, 32 (1985).
[6] X. Zhang, C.-L. Zou, L. Jiang, and H. X. Tang, Phys. Rev. Lett. **113**, 156401 (2014).
[7] Y. Tabuchi, S. Ishino, T. Ishikawa, R. Yamazaki, K. Usami, and Y. Nakamura, Phys. Rev. Lett. **113**, 083603 (2014).
[8] Y. Tabuchi, S. Ishino, A. Noguchi, T. Ishikawa, R. Yamazaki, K. Usami, and Y. Nakamura, Science **349**, 405 (2015).
[9] Y. Cao, P. Yan, H. Huebl, S. T. B. Goennenwein, and G. E. W. Bauer, Phys. Rev. B **91**, 094423 (2015).
[10] B. Bhoi, T. Cliff, I. S. Maksymov, M. Kostylev, R. Aiyar, N. Venkataramani, S. Prasad, and R. L. Stamps, J. Appl. Phys. **116**, 243906 (2014).
[11] D. Xiao, M.-C. Chang, and Q. Niu, Rev. Mod. Phys. **82**, 1959 (2010).
[12] M.-C. Chang and Q. Niu, Phys. Rev. B **53**, 7010 (1996).
[13] G. Sundaram and Q. Niu, Phys. Rev. B **59**, 14915 (1999).
[14] K. Y. Bliokh and Y. P. Bliokh, Phys. Rev. E **70**, 026605 (2004).
[15] M. Onoda, S. Murakami, and N. Nagaosa, Phys. Rev. Lett. **93**, 083901 (2004).
[16] K. Y. Bliokh and Y. P. Bliokh, Phys. Rev. Lett. **96**, 073903 (2006).
[17] M. Onoda, S. Murakami, and N. Nagaosa, Phys. Rev. E **74**, 066610 (2006).
[18] F. D. M. Haldane and S. Raghu, Phys. Rev. Lett. **100**, 013904 (2008).
[19] S. Raghu and F. D. M. Haldane, Phys. Rev. A **78**, 033834 (2008).
[20] Y. Onose, T. Ideue, H. Katsura, Y. Shiomi, N. Nagaosa, and Y. Tokura, Science **329**, 297 (2010).
[21] R. Matsumoto and S. Murakami, Phys. Rev. B **84**, 184406 (2011).
[22] R. Matsumoto and S. Murakami, Phys. Rev. Lett. **106**, 197202 (2011).
[23] A. Okamoto and S. Murakami, Phys. Rev. B **96**, 174437 (2017).
[24] L. Zhang, J. Ren, J.-S. Wang, and B. Li, Phys. Rev. B **87**, 144101 (2013).
[25] R. Shindou, J.-i. Ohe, R. Matsumoto, S. Murakami, and E. Saitoh, Phys. Rev. B **87**, 174402 (2013).
[26] R. Shindou, R. Matsumoto, S. Murakami, and J.-i. Ohe, Phys. Rev. B **87**, 174427 (2013).
[27] D. Jin, L. Lu, Z. Wang, C. Fang, J. D. Joannopoulos, M. Soljačić, L. Fu, and N. X. Fang, Nat. Commun. **7**, 13486 (2015).
[28] D. Jin, Y. Xia, T. Christensen, M. Freeman, S. Wang, K. Y. Fong, G. C. Gardner, S. Fallahi, Q. Hu, Y. Wang, L. Engel, Z.-L. Xiao, M. J. Manfra, N. X. Fang, and X. Zhang, Nat. Commun. **10**, 4565 (2019).
[29] T. Karzig, C.-E. Bardyn, N. H. Lindner, and G. Refael, Phys. Rev. X **5**, 031001 (2015).

[30] S. Park and B.-J. Yang, Phys. Rev. B **99**, 174435 (2019).
[31] S. Zhang, G. Go, K.-J. Lee, and S. K. Kim, Phys. Rev. Lett. **124**, 147204 (2020).
[32] G. Go, S. K. Kim, and K.-J. Lee, Phys. Rev. Lett. **123**, 237207 (2019).
[33] S. Park, N. Nagaosa, and B.-J. Yang, Nano Lett. **20**, 2741 (2020).
[34] P. Shen and S. K. Kim, Phys. Rev. B **101**, 125111 (2020).
[35] A. Okamoto, S. Murakami, and K. Everschor-Sitte, Phys. Rev. B **101**, 064424 (2020).
[36] A. I. Akhiezer, V. G. Bar'yakhtar, and S. V. Peletminskii, *Spin waves* (North-Holland Pub. Co., Amsterdam, 1968).
[37] D. D. Stancil and A. Prabhakar, *Spin Waves* (Springer, New York, 2009).
[38] F. Morgenthaler, IEEE Trans. Magn. **8**, 130 (1972).
[39] N. E. Buris and D. D. Stancil, IEEE Trans. Microwave Theory Tech. **33**, 484 (1985).
[40] D. A. Fishman and F. R. Morgenthaler, J. Appl. Phys. **54**, 3387 (1983).
[41] D. J. Thouless, M. Kohmoto, M. P. Nightingale, and M. den Nijs, Phys. Rev. Lett. **49**, 405 (1982).
[42] M. Kohmoto, Ann. Phys. **160**, 343 (1985).
[43] B. I. Halperin, Phys. Rev. B **25**, 2185 (1982).
[44] S. R. Seshadri, Proc. IEEE **58**, 506 (1970).
[45] A. Prabhakar and D. D. Stancil, IEEE Trans. Magn. **32**, 1918 (1996).
[46] A. F. Cash and D. D. Stancil, IEEE Trans. Magn. **32**, 5188 (1996).
[47] P. K. Tien, Appl. Opt. **10**, 2395 (1971).
[48] M. Mohseni, R. Verba, T. Brächer, Q. Wang, D. A. Bozhko, B. Hillebrands, and P. Pirro, Phys. Rev. Lett. **122**, 197201 (2019).